Open Research Online

The Open University's repository of research publications
and other research outputs

Modelling CDA mass spectra

Journal Item

For guidance on citations see FAQs.

Version: [not recorded]

oro.open.ac.uk

ELSEVIER

Modelling CDA mass spectra

Jon K. Hillier[a],*, N. McBride[a], S.F. Green[a], S. Kempf[b], R. Srama[b]

[a]*Planetary and Space Sciences Research Institute, The Open University, Walton Hall, Milton Keynes, MK7 6AA, UK*
[b]*Max-Planck-Institut für Kernphysik, Saupfercheckweg 1, 69117 Heidelberg, Germany*

Abstract

We present the initial results from a simulation of ion behaviour within Cassini's cosmic dust analyser (CDA) instrument, using an in-house ion dynamics code. This work is to enable and enhance the detailed interpretation of dust impact ionisation mass spectra returned from the Saturnian system. Early work has already provided insights into the properties of the impact plasma in both low- and high-velocity impacts. We find that the isotropic emission of ions from the impact plasma successfully reproduces features seen in flight spectra and that the emitted ions have a higher range of energies (tens to hundreds of eV) than previously reported in some studies. Using these new ion characteristics, we have successfully modelled CDA flight mass spectra.
© 2006 Elsevier Ltd. All rights reserved.

1. Introduction

The cosmic dust analyser (CDA, Srama et al., 2004), on board the Cassini spacecraft, is capable of measuring the flux, mass, velocity, charge and composition of dust particles that enter it. Data from CDA contribute to the understanding of the source, dynamics, evolution and physical and chemical properties of dust particles in the Saturnian system. The composition of the dust particles is measured by the chemical analyser (CA) subsystem—an impact ionisation mass spectrometer. To aid the calibration and interpretation of CA mass spectra, as well as investigate the effect of the ions' initial velocity distribution on spectral peak shapes, it is necessary to model the trajectory of ions within CDA, under a variety of instrument configurations and different impact plasma conditions.

The CA is composed of four sections (Fig. 1A–D) corresponding to the four regions of differing electric field strengths within the instrument. Dust particles initially impact a 0.17-m diameter rhodium target plate (the chemical analyser target, CAT), which is held at approxi-

mately 1000 V (this voltage can be changed during flight) with respect to a copper–beryllium grid approximately 0.003 m above it (forming region A). The resulting $333 \, kV \, m^{-1}$ mean E field rapidly separates any impact plasma, accelerating the cations into the 'drift' region (B) and any anions, together with the electrons, onto the CAT. The charge collected by the CAT is recorded as the QC signal whilst the charge collected by the acceleration grid (68% transmissivity) is recorded as the QA signal. Cations entering the drift region are slowly accelerated over 0.1924 m by a weak ($1.8 \, kV \, m^{-1}$ on average) focussing field generated by the focussing grids (held at approximately −350 V). The outer and inner focussing grids have transmissivities of 90% whereas the central grid has a transmissivity of only 50% and it is from this grid that the QI ion charge signal is collected. All three grids (separated by 0.005 m) are at the same potential, making this region (C) the only true drift region within the CA. Collisions with the grids separating the different field regions are responsible for the majority of the ion losses (72.46%, assuming no losses to other parts of CDA). In the final region (D), the remaining cations are accelerated by a stronger E field ($88.8 \, kV \, m^{-1}$ on average) over 0.027 m into the first plate of the ion detector (the multiplier). The multiplier signal (QM) is sampled at 100 MHz for the first

*Corresponding author. Tel.: +44 1908 659507.
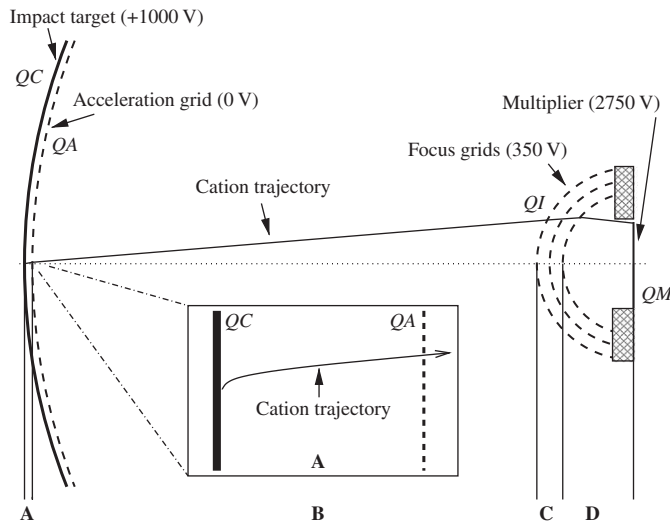*E-mail address:* j.k.hillier@open.ac.uk (J.K. Hillier).

Fig. 1. A 2D schematic of the chemical analyser subsystem of CDA. The dotted line indicates the axis of symmetry (z-axis). Shown are the four main field regions of the CA and the recorded instrument channels (see main text), together with a typical 'just detected' cation trajectory. The inset shows the cation trajectory within the strong field acceleration region, A.
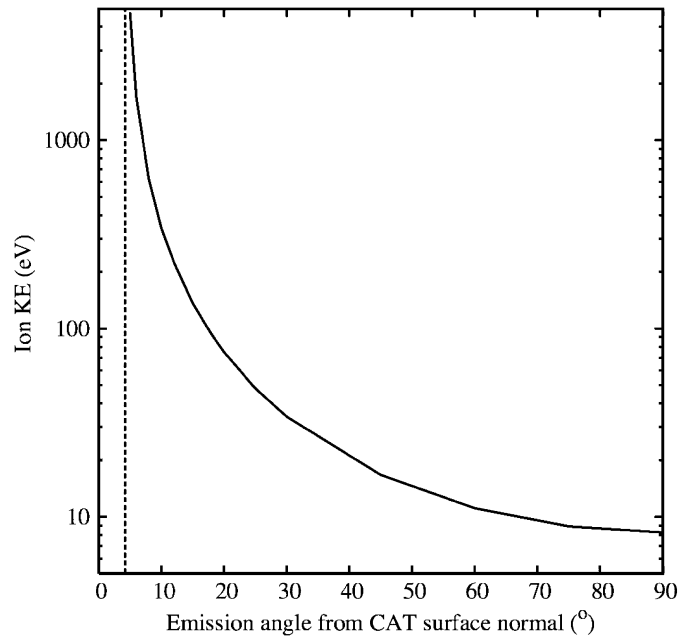

Fig. 2. Maximum energy of ions that will still be detected by the multiplier when emitted at different angles from the CAT surface normal (solid line). The dashed line, at 4.2°, shows the emission angle below which all ions will be detected, regardless of their kinetic energy.

6.4 μs after the instrument is triggered and then at 10 MHz for a further 38.4 μs.

The resulting time of flight (TOF) mass spectrum thus comes from the QM signal. Instrument recording is triggered when the charge signal exceeds a predetermined threshold on the QC, QA, QI or QM channels. In impacts that generate a very small amount of charge, recording is most often triggered by the QM channel, in which case the first peak in the spectrum is missing or truncated.

Although there is some ion focussing in the CA (primarily by the initial acceleration region), the fields within CDA are weak enough that the ions' initial velocities (before any acceleration by the applied E fields) affect their trajectories within the instrument. This means that ions with high enough initial kinetic energies, travelling in a particular direction, may miss the multiplier and instead impact the multiplier housing, the instrument side walls or pass out through the front aperture of CDA. Using a low-resolution (0.1-mm grid size) 2D model of the CA in Simion 3D (Dahl, 2000), it is possible to determine the maximum initial kinetic energy (KE), for ions ejected at different angles from the impact site, which still allows the ions to reach the multiplier.

Fig. 2 shows the result for typical flight instrument voltages and geometry (1020 V acceleration voltage, −339 V focussing voltage, −2740 V multiplier voltage and 0.003 m CAT grid separation, rather than the nominal design voltages of 1000, −350 and −2750 V, respectively). The low angle asymptote occurs when the ions are initially ejected directly towards the multiplier. Ions with emission angles at 90° to the target normal will not be detected if they have a KE of more than 8.26 eV, whereas for an emission angle of 45° this increases to 16.7 eV.

The initial ion velocity distribution (i.e. energy and angular emission distribution) not only affects the likelihood of the multiplier detecting the ions but also affects the shape of the peaks within the TOF mass spectra. CDA does not utilise a reflectron, such as that used by CIDA (Kissel et al., 2003) on board NASA's Stardust, to reduce the effect of the ions' initial velocity distribution on the spectral peaks. CDA therefore produces spectral peaks that are broadened and sometimes shifted within spectra in relation to other peaks, complicating the calibration and interpretation of the mass spectra.

TOF mass spectra are usually calibrated using the relation

$$t_i = a\sqrt{m_i} + b, \tag{1}$$

where t_i is the detection time of an ion of species 'i' and mass m_i with zero initial energy. The zeropoint offset b is related to the trigger time of the instrument and the 'stretch' parameter a is related to instrument geometry and field strengths. In CDA, the measured arrival times of the ions are complicated by their initial velocity distribution, together with the unknown trigger time. However, if it is assumed that the maxima of peaks in a single spectrum correspond to ions with the same energy, and the parent species for at least two peaks can be reliably identified, then it is possible to determine effective values of the a and b parameters easily for a particular spectrum and hence identify the parent species of other spectral peaks.

Fig. 3 shows a typical flight mass spectrum featuring high-energy (hundreds of eV) ions. The Rh$^+$ (target material) peak (at ~4.3 μs) clearly shows broadening
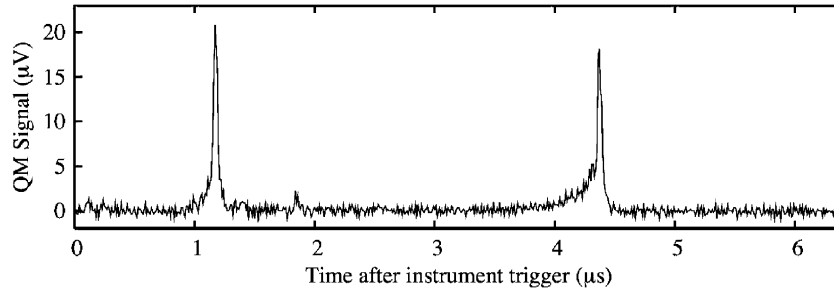
Fig. 3. A typical CA mass spectrum generated by a high-velocity particle impact. Clearly visible peaks (from left to right, at 1.2, 1.8 and 4.3 μs) correspond to carbon, sodium and rhodium cations. This impact was registered on 2 October 2000 and triggered recording on the QM channel, resulting in the loss of the hydrogen cation peak.

towards shorter ion flight times, confirming the existence of high-energy ions within the initial impact plasma. It is worth noting that these spectra are deceptive when shown on a mass scale as they appear to indicate the presence of ion species that are not actually present (i.e. single mass species produce peaks covering many amu), thus we will always present spectra as a function of time.

Whilst Simion 3D is good for modelling individual regions of CDA, it was found to be unsuitable for holistic simulations of the entire CA subsystem of CDA. Software to perform such modelling was instead developed using Research Systems' IDL language. We note, however, that Simion 3D was still used for testing the validity of this model under more restrictive conditions—specific regions of CDA for example. The resulting Cosmic Dust Analyser Chemical Analyser Diagnosis (CDACAD) code models ion dynamics within CDA using a velocity-verlet (Swope et al., 1982) algorithm to solve the ion's equation of motion under the influence of the various E fields within CDA. The continuous E fields used within CDACAD are based upon either simple analytic solutions (e.g. parallel plate in the acceleration region, Fig. 1A) or on fits to Simion 3D models of individual sections of the instrument (Fig. 1B and D). A comparison between 3D CDACAD ion flight times and flight times from Simion models of the central region of CDA is shown in Fig. 4. The apparently large percentage difference in the 1 amu ion flight times is due to the simulated sampling resolution of CDA in CDACAD, resulting in a time resolution of 0.01 μs. All ions flown in the comparison had no initial KE and were released from the centre of the CAT.

In CDACAD, the ions' initial velocity distributions are defined by independently assigning the emission direction distributions and the energy distributions of the ions. The emission direction distributions are divided into an elevation distribution (θ being the angle from the target surface normal) and an azimuthal (φ) distribution. The distribution functions are not continuous but are instead represented by 18 bins ($5°$ and $20°$ wide for θ and φ, respectively) with the population of each bin assigned as required. The geometry of CDA is such that particles can only impact the CAT at angles of less than $28°$ (from the surface normal), so we do not expect significant aniso-
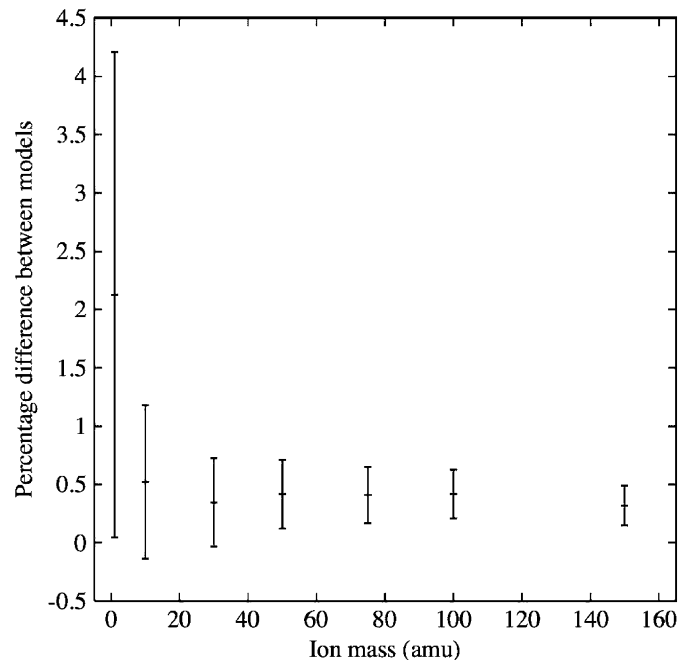

Fig. 4. A comparison of ion flight times from Simion 3D and CDACAD. The absolute percentage difference in the (zero initial KE) ion flight times is shown as a function of the ion mass, in atomic mass units. The Simion calculated flight times were longer than the CDACAD flight times, with the resulting percentage differences calculated by $\mathrm{diff} = 100([t_{\mathrm{Simion}} - t_{\mathrm{CDACAD}}]/t_{\mathrm{CDACAD}})$. The flight time difference for 100 amu ions corresponds to a calculated mass difference of 0.8 amu, using Eq. (1) with $a = 0.48$ and $b = 0$.

tropies in the azimuthal distribution. In subsequent analyses in this paper, we use a uniform distribution in azimuth. The emission angles *within* each bin are assigned using a uniform random distribution. The ion energies are assigned using 20 equal width bins between user-specified minimum and maximum energy boundaries. The energies *within* each bin are assigned using a uniform random distribution to reduce quantisation effects between bins. Some instrument parameters at the time of an impact, such as the various voltages, are known to a good accuracy (± 5 to ± 20 V) for each impact (which, for example, corresponds to a maximum variation in flight time of 0.04 μs ($<1\%$) for a Rh ion), whilst others, such as the CAT-grid

separation distance at the (unknown) dust impact position, vary between known limits. Both the voltages and CAT-grid distance can be varied in CDACAD.

CDACAD is designed to simulate the ion trajectories after plasma dissipation, rather than simulating the behaviour of the impact plasma itself. Spectra generated by CDACAD, and their corresponding energy and emission angle distributions, offer an insight into possible plasma conditions during impacts, rather than providing a unique solution and care must be taken when choosing the initial ion distributions.

2. Results

Unless otherwise indicated, all simulations were performed using the following settings, which are representative of the actual flight settings: CAT voltage = 1020 V, focussing voltage = −339 V, multiplier voltage = −2740 V, CAT-grid distance = 0.00263 m and the impact position on the centre of the CAT.

Using simple isotropic emission angle (θ and φ) distributions, we first compare the peaks generated by Rh^+ ions with zero initial KE and then energies of 0–20 eV (Fig. 5). In the case of the non-zero energy distribution, the ions are equally distributed between the upper and lower energy boundaries.

As may perhaps be predicted from Fig. 2, we find that the last ions to reach the multiplier are not those with zero initial KE, but are in fact due to ions with non-zero energies, emitted at large angles from the surface normal. For particular combinations of ion energy and angular emission angle, the increased velocity component towards

the multiplier (and hence reduction in flight time) is outweighed by the increase in flight path distance due to the tangential velocity component. This flight path difference results in ions with non-zero initial energies and high emission angles taking longer to reach the multiplier than those with zero initial energy that, by definition, travel directly towards the multiplier. The ions that reach the multiplier first are the subset of high-energy ions released at angles close to or along the surface normal.

Using the same isotropic emission distributions we now investigate the effect of changing the lower energy boundary of the energy distribution on the position of both the tail of the peak and the peak maximum. In Fig. 6, we can see the effect of keeping the highest available energy fixed at 50 eV whilst raising the lower energy boundary from 0 to 50 eV in 10 eV steps. The ion energies are once again distributed evenly between the boundaries. Changing the low energy boundary results in a significant shift of the position of the peak maximum, as well as reducing the number of ions detected and changing the peak shape itself. If the lower energy boundary is kept fixed and the higher energy boundary increased (Fig. 7), we see that the maximum of the peak remains in the same position.

With increasing maximum ion energies, the area under the peak decreases because a higher proportion of ions fail to reach the multiplier. Despite the reduction in peak amplitude, the relative shape of the peaks near their maxima remains similar, with the major changes occurring in the leading edge of the peaks. These early arrival times can *only* result from high-energy ions and this is what we see in data from high-velocity impacts (Fig. 3). However, little can be said about the detailed energy and angular
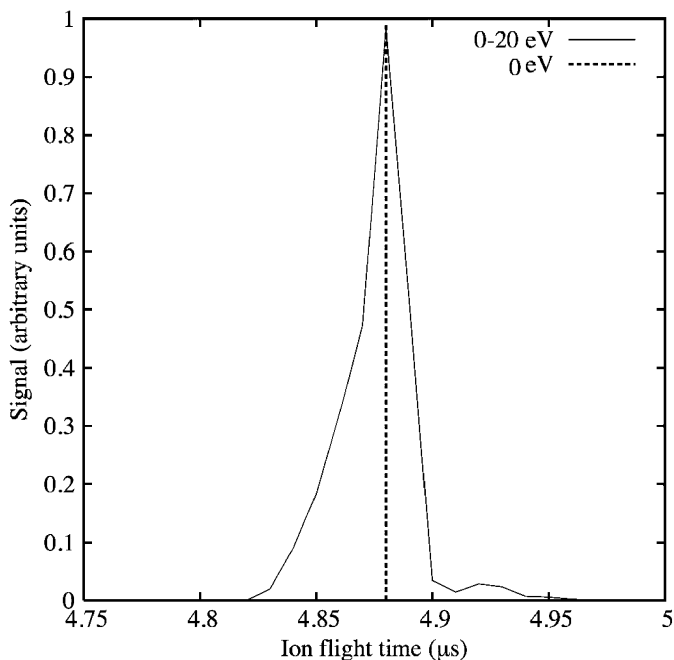

Fig. 5. A simulated rhodium ion peak, showing that the ions with non-zero energies contribute to extending the peak past the zero energy position (dashed line).
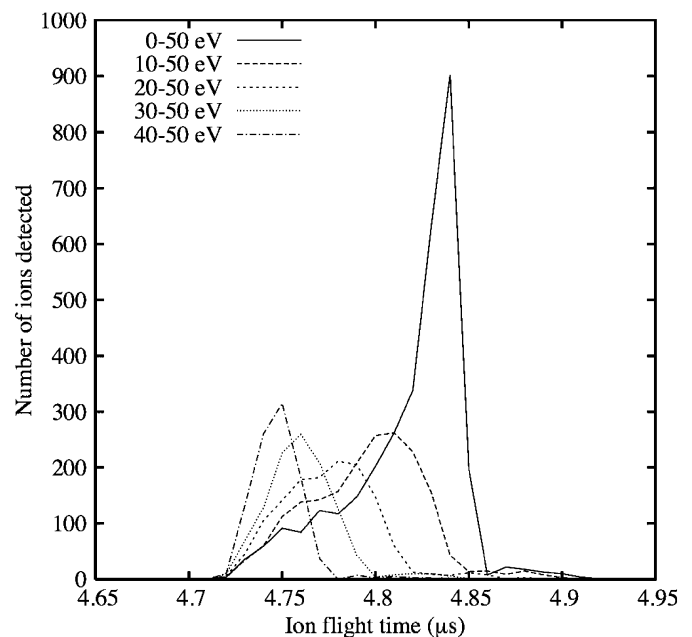

Fig. 6. Simulated rhodium peaks from ions with different initial energy ranges. The same number of ions (10,000) were flown in each case.
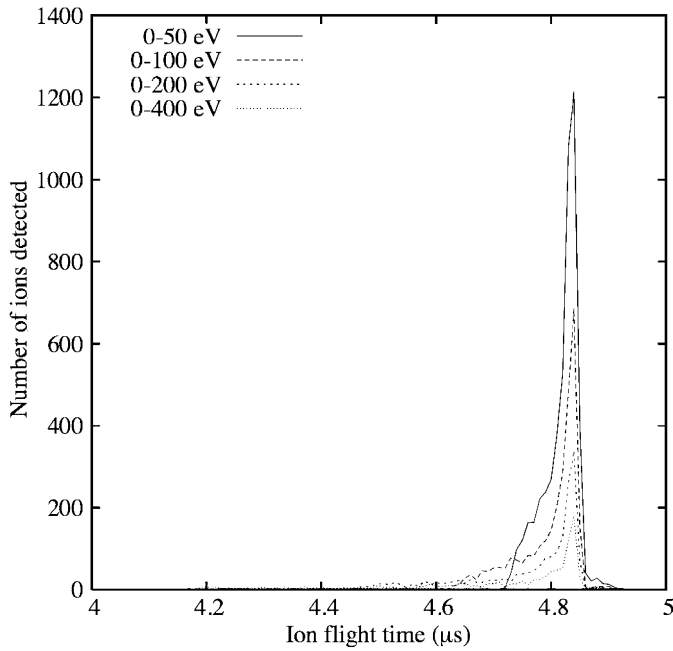
Fig. 7. Rhodium peaks resulting from groups of ions with different maximum energies. The 0–400 eV peak extends as far forward as 4.2 μs. No vertical scaling has been applied.
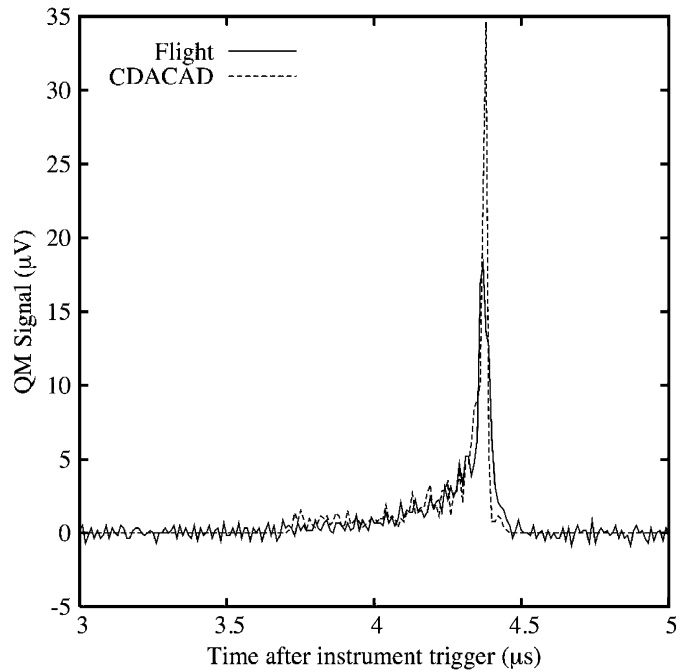

Fig. 8. A comparison of the simplest possible CDACAD model fit to a flight rhodium peak; 15,000 ions were flown in the CDACAD model and the resulting peak has been vertically scaled to fit the rising flank of the flight peak.
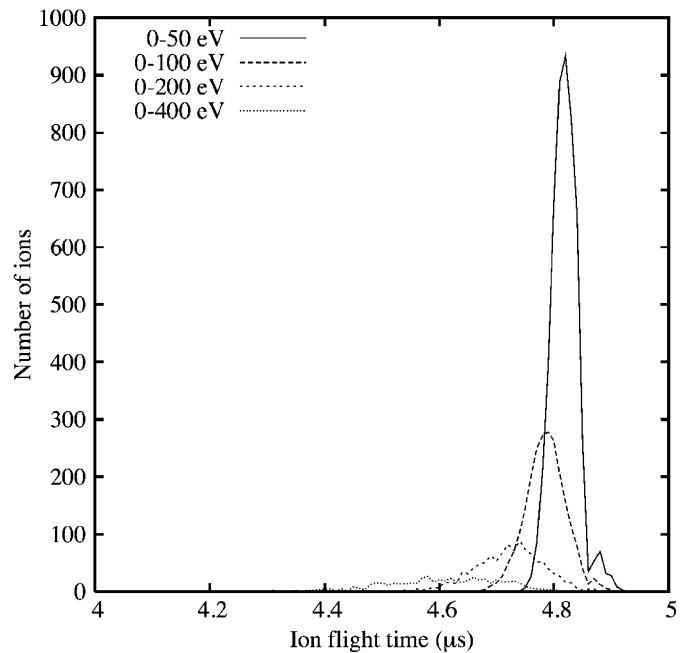

Fig. 9. CDACAD simulated rhodium peaks using Maxwell–Boltzmann energy distributions; 10,000 ions were flown to create each peak and no vertical scaling has been applied. Ion energies shown are lower and upper limits.

distributions of these ions because their detection (arrival at the multiplier) is so strongly determined by the instrument geometry and field strengths. Consequently, for the high-energy ions, only those emitted close to the surface normal are detected (Fig. 2).

Fig. 8 shows the result of a simplest-case model of the Rh peak in Fig. 3. Here, we assume isotropic angular emission distributions, as before, and an energy distribution in which the ions are equally distributed between 0 and 400 eV. The overall peak shape in this spectrum is clearly dominated by the effects of CDA's geometry and fields although there are some discrepancies. The simulated peak amplitude is too high in comparison with the rising flank of the peak, whilst there appears to be a deficit in the trailing flank of the peak. These factors indicate a more complex energy distribution, with a greater fraction of ions towards the higher end of the energy range, in the flight spectrum. Although not likely for a plasma under these conditions (rapidly expanding in a strong E field), we then use a Maxwell–Boltzmann (MB) energy distribution, corresponding to a plasma in Local Thermodynamic Equilibrium (LTE). Fig. 9 demonstrates the peak shapes created when using MB distributions for the energy distributions. The four cases shown correspond to plasma temperatures of 125,000–1,000,000 K. Whilst the MB distribution produces a better fit for the trailing flank, the high-energy ions (leading flank) appear depleted. This suggests that the actual energy distribution will lie somewhere between the equally distributed and MB distributions.

Finally, still using isotropic angular emission, and an MB energy distribution with a maximum energy of 80 eV (modal energy ~27.5 eV, corresponding to a plasma temperature of 300,000 K), we model a more complex spectrum. Spectra from low-velocity impacts of ice-rich dust (or onto water ice targets (Timmermann and Grün, 1991)) show periodic spectral features characteristic of
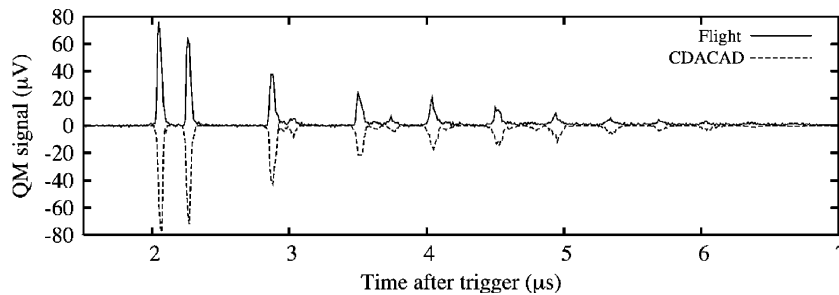
Fig. 10. A CDACAD simulation of a more complex water-cluster spectrum. The hydrogen peak has been truncated in the flight spectrum, with the first peak (2.1 μs) due to hydronium (H_3O^+) ions. The rhodium peak is barely visible and occurs at approximately 4.8 μs. For examples of similar spectra, see Hillier et al. (2006).

water clusters (in cation spectra, these features correspond to $H(H_2O)_n^+$). Using CDACAD, we simulate the behaviour of a plasma containing water clusters up to $n = 10$, as well as sodium-water clusters, silicate-related species and rhodium (Fig. 10). The upper spectrum in Fig. 10 was created by a small (~1 μm diameter) mostly water ice particle impacting at approximately 6 km s^{-1} within the Saturnian system. The CDACAD spectrum fits this flight spectrum well.

3. Discussion

Although still at an early stage, the modelling of ion dynamics within CDA has been shown to be successful in recreating many of the features seen in flight spectra. Ions ejected over a variety of angles from the CAT surface normal, with high energies, produce spectral features whose shapes are dominated by the response function of the CA (Fig. 3). This instrument behaviour can be successfully modelled, revealing information about the impact plasma conditions which would have been lost had CDA used a reflectron to perform strict ion energy discrimination.

Modelling peak shapes using a variety of energy distributions shows that the right-hand flank of a peak (the 'tail'), where the peak disappears into the background noise, is least affected by changes in the ion energy distribution. This suggests that, when coadding spectra to hunt for low abundance, unrelated species, the best results will be obtained if the individual spectra are aligned using the position of the 'tails' rather than the position of the peak maxima. If searching for species that are suspected to have similar energy distributions (such as cluster ions), then aligning on the peak maxima should be more suitable.

As most flight spectra exhibit the characteristic 'tail' feature, and can be modelled well by assuming isotropic angular emission, it appears that at least for the high-velocity impacts (those resulting in appreciable numbers of ions with energies of hundreds of eV), there is no large-scale focussing of ions in the direction of the target normal. In fact, if we apply *narrow* ion angular emission distribution functions such as $\cos^3(\theta)$ (Ratcliff and Allahdadi,

1996), we produce peaks which are *broader* than those observed in CDA flight spectra. Furthermore, the pronounced 'tail' of the peaks is not produced. This is because with this distribution, the relative increase in the number of ions ejected towards the multiplier increases the number of high-energy ions detected, widening the spectral peak towards shorter flight times, whilst the number of ions ejected at high angles from the surface normal is reduced, resulting in fewer ions following trajectories which allow them to arrive after the zero initial energy ions, so removing the tail of the peak.

The range of ion energies required to fit peaks in the flight spectra is greater than previously reported in some laboratory experiments. For higher-velocity impacts, our results are in good agreement with both Ratcliff and Allahdadi (1996) and Hornung et al. (1996), with ion energies of hundreds of eV. For the low-velocity impacts (< 10 km s^{-1}), which produce cluster ion spectra, we obtain good fits to the data using ion energies of up to ~80 eV, contrasting with the results of Friichtenicht, quoted by Ratcliff and Allahdadi (1996), of 0.5 eV for metallic target ions (impact velocities of 17–47 km s^{-1}). The ion energies we derived for low-velocity impacts do, however, agree with those found by Burchell et al. (1996) of tens of eV and we remain unable to explain the discrepancy with Friichtenicht's results. In the case of the CDACAD simulations of the low-velocity cluster spectra, we used a MB energy distribution, which would be appropriate for plasma in LTE. The derived plasma temperatures from these simulations are extremely high (hotter than those found by Smith and Adams (1973) of 2000–4000 K for impact velocities of up to 10 km s^{-1}), whilst the existence of cluster ions implies a low-temperature plasma. The plasma is thus unlikely to be in LTE and the choice of MB distributions is probably not the most physically realistic. However, we note that similar results (spectral features) could be obtained using a suitably centred broad Gaussian energy distribution. Our model fits show that plasma produced by extremely high-velocity impacts also contains significant numbers of ions with such high energies that an impact plasma consisting solely of thermal ions is unlikely and such a plasma may be better described by a two-component model with a population of

high-energy non-LTE ions and a smaller population of ions in approximate LTE.

Development of CDACAD is underway to simulate modifications to ion flight times due to further plasma effects such as debye shielding or delayed ionisation. CDACAD should also prove to be useful in investigating the efficiency of ion production by allowing estimates of ion losses to other parts of CDA for different plasma conditions. As Cassini continues its tour of the Saturnian system, CDA is returning a large number of mass spectra, generated by dust with a large range of velocities and masses. Modelling the spectra produced by these impacts may enable correlations between dust mass and velocity and the impact plasma conditions to be better understood, providing a further way to determine these dust properties. It will also be possible to investigate any potential differences in energy or emission distributions between ions from impacting projectiles and ions from the CAT materials.

4. Conclusions

From the development and use of the CDACAD program we conclude:

(1) The model is able to produce synthetic spectra which match CDA flight spectra, whilst being quicker to configure and use than Simion 3D. The main advantages over Simion 3D are the absence of spatial quantisation in CDACAD and the ability to change instrument geometry instantly.
(2) Spectral peak shapes are found to be dominated by the angular/energy response of CDA. As a consequence, many observed peak shapes (particularly in the trailing flank of peaks) require broader source functions for the ion emission angular distributions, rather than the narrow distributions (e.g. ion focussing along the target surface normal) used by others. Indeed, the distributions derived in Ratcliff and Allahdadi (1996) varied according to the energy of the ion species, implying that the instrument configuration (and hence response function) used in their experiment was dominating the shape of their spectral peaks.
(3) We find that a wide range of ion energies (up to hundreds of eV) are required to fit peaks seen in flight spectra, and that this is independent of any assumption about the ions' angular distribution. Features found to be indicative of ion energies of tens of eV are seen even in low-velocity ($<10 \, \mathrm{km \, s^{-1}}$) impacts, contrary to some previously reported laboratory studies.

(4) The range of ion energies seen in flight spectra, together with the presence of cluster ions, implies that the impact plasma is either not in LTE or remains in LTE for a negligible time.

References

Burchell, M.J., Kay, L., Ratcliff, P.R., 1996. Use of combined light flash and plasma measurements to study hypervelocity impact processes. Adv. Space Res. 17 (12), 141–145.

Dahl, D.A., 2000. Simion for the personal computer in reflection. Int. J. Mass Spectrom. 200, 2–25.

Hillier, J.K., Green, S.F., McBride, N., Schwanethal, J.P., Srama, R., Kempf, S., Postberg, F., McDonnell, J.A.M., Grün, E., 2006. The composition of Saturn's E ring. MNRAS, submitted for publication.

Hornung, K., Malama, Y.G., Thoma, K., 1996. Modeling of the very high velocity impact process with respect to in situ ionization measurements. Adv. Space Res. 17 (12), 77–86.

Kissel, J., Glasmachers, A., Grün, E., Henkel, H., Höfner, H., Haerendel, G., Von Hoerner, H., Hornung, K., Jessberger, E.K., Krueger, F.R., Möhlmann, D., Greenberg, J.M., Langevin, Y., Silén, J., Brownlee, D., Clark, B.C., Hanner, M.S., Hoerz, F., Sandford, S., Sekanina, Z., Tsou, P., Utterback, N.G., Zolensky, M.E., Heiss, C., 2003. Cometary and Interstellar dust analyzer for comet Wild 2. J. Geophys. Res. 108 (E10), 4-1–4-8.

Ratcliff, P.R., Allahdadi, F., 1996. Characteristics of the plasma from a $94 \, \mathrm{km \, s^{-1}}$ micro-particle impact. Adv. Space Res. 17 (12), 87–91.

Smith, D., Adams, N.G., 1973. Studies of plasma production at hypervelocity microparticle impact. J. Phys. D: Appl. Phys. 6, 700–719.

Srama, R., Ahrens, T.J., Altobelli, N., Auer, S., Bradley, J.G., Burton, M., Dikarev, V.V., Economou, T., Fechtig, H., Görlich, M., Grande, M., Graps, A., Grün, E., Havnes, O., Helfert, S., Horanyi, M., Igenbergs, E., Jessberger, E.K., Johnson, T.V., Kempf, S., Krivov, A.V., Krüger, H., Mocker-Ahlreep, A., Moragas-Klostermeyer, G., Lamy, P., Landgraf, M., Linkert, D., Linkert, G., Lura, F., McDonnell, J.A.M., Möhlmann, D., Morfill, G.E., Müller, M., Roy, M., Schäfer, G., Schlotzhauer, G., Schwehm, G.H., Spahn, F., Stübig, M., Svestka, J., Tschernjawski, V., Tuzzolino, A.J., Wäsch, R., Zook, H.A., 2004. The Cassini cosmic dust analyzer. Space Sci. Rev. 114 (1–4), 465–528.

Swope, W.C., Andersen, H.C., Berens, P.H., Wilson, K.R., 1982. A computer simulation method for the calculation of equilibrium constants for the formation of physical clusters of molecules: application to small water clusters. J. Chem. Phys. 76 (1), 637–649.

Timmermann, R., Grün, E., 1991. Plasma emission from high velocity impacts of microparticles onto water ice. In: Levasseur-Regourd, A.C., Hasegawa, H. (Eds.), Origin and Evolution of Interplanetary Dust. Kluwer Academic Publishers, Dordrecht, pp. 375–378.